

1 Salt intrusion dynamics in a well-mixed sub-estuary connected to a
2 partially to well-mixed main estuary

3 Zhongyuan Lin^{c,d}, Guang Zhang^{a,b}, Huazhi Zou^{c,d}, Wenping Gong^{a,b*}

4 ^aSchool of Marine Sciences, Sun Yat-sen University, Zhuhai, 519082, China

5 ^bGuangdong Provincial Key Laboratory of Marine Resources and Coastal Engineering, Zhuhai,
6 519082, China

7 ^c Key Laboratory of Pearl River Estuary Regulation and Protection of Ministry of Water
8 Resource, Guangzhou 510611, China

9 ^d Pearl River Water Resource Research Institute, Guangzhou 510611, China

10
11 Corresponding Author: Wenping Gong (gongwp@mail.sysu.edu.cn)
12

13
14 **Abstract**
15

16 Salt intrusion in estuaries has been exacerbated by climate change and human
17 activities. Previous studies have primarily focused on salt intrusion in the mainstem of
18 estuaries, whereas those in sub-estuaries (those branch off their main estuaries) have
19 received less attention. During an extended La Niña event from 2021 to 2022, a sub-
20 estuary (the East River estuary) alongside the Pearl River Estuary, China, experienced
21 severe salt intrusion, posing a threat to the freshwater supply in the surrounding area.
22 Observations revealed that maximum salinities in the main estuary typically preceded
23 spring tides, exhibiting significant asymmetry in salinity rise and fall over a fortnightly
24 timescale. In contrast, in the upstream region of the sub-estuary, the variation of salinity
25 was in phase with that of the tidal range, and the rise and fall of the salinity were more
26 symmetrical.

27 Inspired by these observations, we employed idealized numerical models and
28 analytical solutions to investigate the underlying physics behind these behaviors. It was

29 discovered that under normal dry condition (with a river discharge of $1500 \text{ m}^3 \text{ s}^{-1}$ at the
30 head of the main estuary), the river-tide interaction and change in horizontal dispersion
31 accounted for the in-phase relationship between the salinity and tidal range in the
32 upstream region of the sub-estuary. Under extremely dry conditions (i.e., a river
33 discharge of $500 \text{ m}^3 \text{ s}^{-1}$ at the head of the main estuary), salinity variations were in-
34 phase with those of the tidal range in the middle as well as the upstream region of the
35 sub-estuary. The variation of salinity in the main estuary, along with those of salt
36 dispersion and freshwater influx inside the sub-estuary collectively influenced salinity
37 variation in the well-mixed sub-estuary. These findings have important implications for
38 water resource management and salt intrusion prevention in the catchment area.

39 **Keywords:** Sub-estuaries; River-tide interaction; Partially to well-mixed estuary.

40

41 **1. Introduction**

42

43 Salt intrusion in estuaries has emerged as an increasingly significant
44 environmental issue, as it contaminates water quality, restricts freshwater supply, and
45 affects the biota's habitat in estuaries (Payo-Payo et al., 2022). The severity of salt
46 intrusion in estuaries has been further exacerbated by both climate change and
47 anthropogenic activities. Climate change has led to more severe droughts in various
48 regions worldwide (Spinoni et al., 2014), resulting in reduced freshwater flow from
49 upstream watershed basin into estuaries. In turn, this has intensified salt intrusion in
50 these areas. Additionally, sea level rise has been identified as a contributing factor to

51 this phenomenon (e.g., Hong et al., 2020). Human activities, including dam
52 construction in the watershed, channel dredging, and land reclamation in estuaries, have
53 caused reductions in river inflow, channel deepening, and enhanced convergence of
54 estuarine geometry, all of which favor an increase in salt intrusion (e.g., Ralston and
55 Geyer, 2019).

56 Salt intrusion in estuaries is the result of landward salt transport, which consists of
57 steady shear and tidal oscillatory transport (MacCready and Geyer, 2010). The
58 combination of estuarine circulation and salinity stratification induces a steady shear
59 when averaged in a tidal cycle. Tidal oscillatory transport is generated by tidal pumping
60 such as the jet-sink flow for an inlet (Stommel and Farmer, 1952), tidal trapping with a
61 side embayment (Okubo, 1973), tidal shear dispersion by the vertical shears of current
62 and mixing (Bowden, 1965), tidal straining (Simpson et al., 1990), and chaotic stirring
63 (Zimmerman, 1986).

64 In general, for a partially mixed estuary in which the steady shear dominates the
65 landward salt transport, the salt intrusion is strongest during neap tides and weakest
66 during spring tides under the steady-state conditions, meaning that the change in salinity
67 is out-of-phase with that in the tidal range. However, for a well-mixed and/or a salt
68 wedge estuary, in which the tidal dispersion is the dominant contributor to landward
69 salt transport, the salt intrusion is strongest during spring tides and weakest during neap
70 tides, signifying that the salinity variation is in phase with the tidal range (Ralston et
71 al., 2010). These steady-state situations are altered by the unsteadiness of external
72 forcing and the adjustment of estuaries to the changing forcings (Chen 2015 and

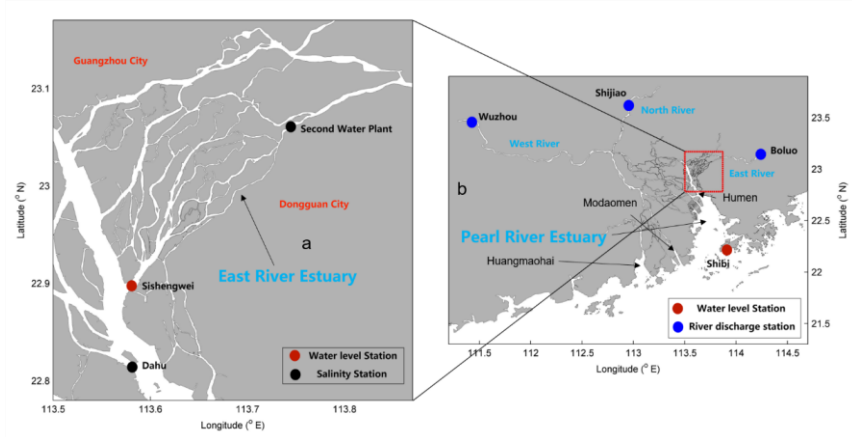
73 references therein). In general, when the internal timescale of an estuary, which is
74 defined as the time needed for a water parcel from the upstream to travel through the
75 estuary by the river-induced flow, is shorter than the external timescale, which is often
76 the spring-neap tidal cycle, the salinity variation in an estuary can keep pace with the
77 change in tidal forcing and reaches steady state. However, when the internal timescale
78 is longer than the external timescale, the salt intrusion can hardly reach the steady state,
79 and there exists a phase shift between the salt intrusion and tidal range, such as in the
80 Modaomen estuary (Gong and Shen, 2011) and Hudson River (Bowen and Geyer,
81 2003).

82 Previous studies on salt intrusion have primarily focused on main estuaries, where
83 freshwater discharge empties into the estuarine waterbody at the estuary head and is
84 profoundly diluted by the seawater from the ocean. However, there has been relatively
85 less research on salinity dynamics specifically in tidal creeks or sub-estuaries, i.e. those
86 that reside aside from their main estuary. It is worth noting that larger estuaries often
87 possess sub-estuaries or tidal creeks, as highlighted by Uncles and Stephens (2010).
88 Sub-estuaries branch off the stem of their main estuary and exhibit behavior that is
89 partially dependent on processes acting within the main estuary. Haywood et al. (1982)
90 described the importance of conditions at the confluence of the York River sub-estuary
91 and the Chesapeake Bay to salinity stratification within the sub-estuary. Uncles and
92 Stephens (2010) investigated the salinity dynamics in a sub-estuary (Tavy) connected
93 to the main estuary (Tamar, UK). They noted that the tidal range had a limited effect on
94 the salinity in the sub-estuary. Yellen et al. (2017) examined the sediment dynamics in

95 a side embayment of the main estuary of Connecticut, USA, and found that salinity
96 intrusion from the main estuary enhanced sediment trapping inside the sub-estuary.

97 The previous studies on sub-estuary salt dynamics have mainly focused on
98 examining salinity variabilities and water column stratification, as exemplified by the
99 work of Haywood et al. (1982). Some investigations have also explored the influence
100 of river discharge from the heads of the main estuary and sub-estuary, as well as the
101 impact of winds, as discussed by Uncles and Stephens (2010). However, there remains
102 a knowledge gap regarding how the salt dynamics in the main estuary affect those in
103 the sub-estuary, as well as how the interaction between river flow and tides influences
104 salinity variations in the sub-estuary. Regarding the river-tide interaction, here we focus
105 on how tides affect river flow through mechanisms such as nonlinear bottom friction
106 and advective terms in the momentum equation, as outlined by Buschman et al. (2009),
107 whereas the effect of river flow on tidal propagation will not be explored.

108 In 2021, under the influence of a La Nina event, the precipitation in the Pearl River
109 Delta (PRD) area (Fig. 1), China, was extremely low, and the salt intrusion was very
110 severe, which imposed a great threat to the freshwater supply in the region, especially
111 during winter months (December to February). Alongside the Pearl River Estuary
112 (PRE), a sub-estuary of the East River estuary (Fig. 1), also experienced strong salt
113 intrusion and heavily impacted the water supply to the city of Dongguan, home to a
114 population of 10 million people. This shortage of freshwater became a significant
115 concern for the surrounding people, especially during the Spring Festival, the Chinese
116 Lunar New Year.



117
 118 Fig.1. a) The East River estuary; b) Map of the Pearl River Delta and the locations of hydrological
 119 and water level stations.
 120

121 The present work has two objectives: (a) to investigate the characteristics of salt
 122 intrusion in a well-mixed sub-estuary by analyzing observation data. The characteristics
 123 include spatial-temporal variations of salt intrusion and its relationship with river flow
 124 and tidal range; (b) to explore the underlying physics behind salt intrusion in the sub-
 125 estuary, such as the impacts of salt dynamics in the main estuary, and the river-tide
 126 interaction inside the sub-estuary. To achieve the above goals, we first collected and
 127 analyzed observational data of salt intrusion at the East River estuary. Then we utilized
 128 an idealized configuration for numerical model investigation. Two numerical model
 129 experiments with mean and extremely low river discharges in dry seasons in the main
 130 estuary, respectively, were conducted to identify the relevant mechanisms for the
 131 variability of salt intrusion in the sub-estuary. Furthermore, to clearly understand the
 132 phase relationship between salinity and tidal range, analytical solutions for the

133 ~~subtidal~~tidally-averaged salinity in the well-mixed sub-estuary were utilized. In this
134 study we set a tidal period to be 25 hours.

135 The remainder of this paper is structured as follows. The study site is briefly
136 introduced in Section 2. The methods of data analysis, numerical model simulation, and
137 analytical solution are presented in Section 3. In Section 4, the results of the salt
138 intrusion dynamics through the measurement data analysis, numerical model, and
139 analytical solution are demonstrated, followed by some discussions on the impacts of
140 river-tide interaction in the sub-estuary, the salt dynamics in the main estuary, and the
141 limitations of this study in Section 5. Finally, a summary and conclusion are given in
142 Section 6.

143

144 **2. Study site**

145

146 The Pearl River, China's second largest river in terms of annual freshwater
147 discharge, has three main branches: West River, North River, and East River (Hu et al.,
148 2011), as displayed in Fig. 1b. The Pearl River forms a complex delta, known as the
149 Pearl River Delta (PRD), which consists of the downstream river network and three
150 estuaries, from west to east: the Huangmaohai Estuary, the Modaomen Estuary, and the
151 PRE (Fig. 1b). The PRE, the largest of the three estuaries, is funnel-shaped and has a
152 mean depth of 4.6 m (Wu et al., 2016). Its width decreases from 50 km at its mouth
153 between Hong Kong and Macau to 6 km at Humen Outlet. The axial length of the
154 estuary from the mouth to Humen is approximately 70 km. Above the Humen, the
155 estuary becomes relatively straight and further extends almost 90 km landward to its

156 head. Upstream of the Humen, there exists a waterway known as Shizhiyang. Along the
157 waterway, there are several river tributaries, among which the East River sub-estuary,
158 are distributed on the east side.

159 The river discharge ~~dumping~~ into the PRE is about 1/4 of the total river flow from
160 the Pearl River. The total annual river ~~discharge-flow~~ of the Pearl River is 3260×10^8
161 m^3 , in which the river ~~discharge-flow~~ experiences distinct seasonal variations. During
162 the dry season (from November to March), the river ~~dischargeflow at the head of the~~
163 ~~Pearl River~~ takes up only about 30% of the ~~total~~ annual ~~dischargeflow~~, ~~so the total river~~
164 ~~discharge of the Pearl Riverwhich~~ is about $6000 \text{ m}^3/\text{s}$ ~~in the dry season~~, and the
165 ~~upstream~~ river discharge ~~intoof~~ the PRE is $1500 \text{ m}^3/\text{s}$ (1/4 of the total). Under extremely
166 dry conditions, the river discharge ~~at the head of~~~~into~~ the PRE can be less than 1000
167 m^3/s .

168 The PRE has a microtidal and mixed semi-diurnal regime (Mao et al., 2004). The
169 annual mean tidal range is 1.45 m near Lantau Island (at the mouth of the PRE) and
170 1.77 m near the Humen outlet (Gong et al., 2018). The amplitudes of M_2 , S_2 , K_1 , and O_1
171 constituents near the Lantau Island are 35.5, 14, 33.5, and 27.9 cm, respectively (Mao
172 et al., 2004), showing the dominance of the M_2 constituent. The alternation of neap and
173 spring tides causes the tidal range near Lantau Island to vary from approximately 0.7 m
174 during neap tides to approximately 2 m during spring tides. Apart from the fortnightly
175 variation of the tidal range, there also exists a monthly variation, which is referred to as
176 the apogee/perigee cycle (Payo-Payo et al., 2022).

177 The PRE exhibits strong seasonal variation and is highly stratified during the wet

178 summer season (July to September), with the bottom isohaline of 10 $\text{psu}/\text{kg}/\text{kg}$
179 protruding into the upper estuary (50 to 70 km from the estuary mouth) and the surface
180 isohaline of 10 $\text{psu}/\text{kg}/\text{kg}$ extending outside of the estuary. The ~~subtidal-tidally-~~
181 averaged bottom-surface salinity difference is mostly greater than 10 $\text{psu}/\text{kg}/\text{kg}$
182 inside the estuary (Dong et al., 2004). During the dry season, the PRE is generally in a
183 partially mixed state, with the bottom isohaline of 10 $\text{psu}/\text{kg}/\text{kg}$ reaching the Humen
184 Outlet, and the surface isohaline of 10 $\text{psu}/\text{kg}/\text{kg}$ lying in the upper estuary (Wong et
185 al., 2003; Gong et al., 2018). In the dry season, the horizontal difference of depth-mean
186 salinity varies by between 20 and 25 $\text{psu}/\text{kg}/\text{kg}$ across a distance of 70 km from the
187 estuary mouth to Humen Outlet, and the vertical salinity difference between the surface
188 and bottom varies from 1 to 12 $\text{psu}/\text{kg}/\text{kg}$ along the channels in the estuary.

189 The East River is a branch of the Pearl River, with a length of 562 km and a
190 drainage area of 27,040 km². It forms a sub-delta, known as the East River Delta, which
191 is located on the east side of the PRE and above the Humen Outlet (Fig. 1a). The upper
192 reach of the East River is essentially composed of a single channel, while in its lower
193 reach, downstream of Dongguan City, a complex river network is formed, including
194 several tributaries (Fig. 1a). Here we focus on the southernmost tributary, which merges
195 into the main estuary at the confluence of Sishengwei, where a hydrological station
196 resides. This tributary has a length of approximately 75 km from the confluence
197 (Sishengwei) to the upstream hydrological station of Boluo (Fig. 1b), and a mean water
198 depth of less than 5 m.

199 The average annual freshwater load of the East River is $240 \times 10^8 \text{ m}^3$, or a mean

200 river discharge of $728 \text{ m}^3 \text{ s}^{-1}$, accounting for 7.1% of the total river flow of the Pearl
201 River. During dry seasons, the river discharge is approximately $400 \text{ m}^3 \text{ s}^{-1}$. However,
202 the annual mean river discharge in 2021 was only $262 \text{ m}^3 \text{ s}^{-1}$. During the winter of 2021,
203 the salinity at several water plants exceeded the drinking water criteria of 0.5
204 ~~psu~~mg/kg for a lasting duration of 3 months and impaired the freshwater supply in
205 the region.

206 Similar to the main estuary, the tidal regime in the East River sub-estuary is a
207 mixed semi-diurnal one, with the tidal range decreasing when propagating upstream
208 due to the predominance of the bottom friction over the estuarine convergence. In recent
209 decades, the tidal strength has been seen to increase by human activities, such as sand
210 mining in the estuary (Jia et al., 2006).

211

212 **3. Methods**

213

214 **3.1 Observation data and analysis**

215

216 The observation data here consist of the daily discharge of the West, North, and
217 East Rivers, hourly water level data at the confluence (Sishengwei) between the East
218 River sub-estuary and the main estuary (PRE), daily sea level at the mouth of the PRE
219 (Shibi), and hourly surface salinity data at the Dahu station, which is located
220 downstream of the Sishengwei, and at the Second Water Plant of Dongguan City. These
221 two stations span a distance of approximately 30 km. The river discharge data at three
222 river branches of the Pearl River, hourly water level data at Sishengwei, and hourly

223 surface salinity data at Dahu are from the Pearl River Water Resources Commission,
224 whereas the salinity data at the Second Water Plant is from the Water Authority of
225 Dongguan City. The sea level data at the estuary mouth is from the Hong Kong
226 Observatory (<http://gb.weather.gov.hk/contentc.htm>). All the salinity data are the
227 surface salinities.

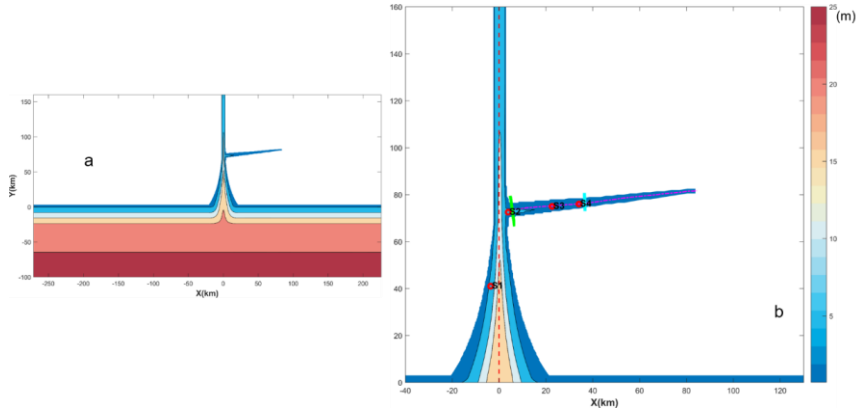
228 The salinity data at the Second Water Plant was subject to wavelet analysis, a
229 method that has been widely used to analyze geophysical data, like in salt intrusion
230 studies in estuaries (Liu et al., 2014; Gong et al., 2022). This method can identify
231 localized periodicities (or bands) that are linked to specific processes, such as tidal and
232 spring-neap variations. In this study, the continuous wavelet transform (CWT) method
233 was used to identify the multi-scale characteristics of salinity, and cross wavelet was
234 employed to examine the nonlinear correlations among variables, such as between the
235 salinity of the Second Water Plant and the water level at Sishengwei, between the
236 salinity of the Second Water Plant and the salinity of Dahu, and between the salinity of
237 the Second Water Plant and the river discharge at the Boluo Station.

238

239 **3.2 Numerical model configuration and experiments**

240

241 The Regional Ocean Modeling System (ROMS) was used in this modeling study.
242 ROMS is a free-surface, hydrostatic, primitive-equations ocean model that uses
243 stretched, terrain-following vertical coordinates and orthogonal curvilinear horizontal
244 coordinates on an Arakawa C-grid (Haidvogel et al. 2000). The model domain was
245 designed as an estuary-shelf system (Fig. 2). In the coordinate system, x is in the



246
 247 Fig. 2. Geometry and bathymetry of the idealized model domain: a)for the whole domain;
 248 b)zoom in for the area of concern. The origin of the coordinates is in the middle of the main
 249 estuary mouth. The longitudinal sections in the main and sub-estuary are shown as dashed lines,
 250 and the cross-sections inside the sub-estuary are shown as color solid lines. The locations of
 251 several stations are indicated.

252
 253 cross-estuary direction, with rightward being positive, y is in the along-channel
 254 direction, with landward being positive, and z directs upward. The origin of the
 255 system is in the middle of the estuary mouth. The estuary is composed of a convergent
 256 part and a straight part. The geometry and bathymetry of the estuary roughly resemble
 257 those of the PRE, with the convergent part extending from the estuary mouth to the
 258 Humen Outlet (70 km in length), and the straight part from the Humen Outlet to the
 259 head of the estuary (90 km long). For the convergent part, the estuarine width B is
 260 assumed to decrease exponentially in the landward direction, as follows:

261
$$B = B_0 \exp\left(-\frac{y}{L_b}\right) \quad (1)$$

262 where B_0 is the estuarine width at the estuary mouth (here taken as 46 km) and L_b is

263 the width convergence length (taken as 31 km, as estimated by Zhang et al., 2021). The
264 bathymetry of the PRE is characterized by deep channels and side shallow shoals.
265 Following Wei et al. (2017), we roughly mimicked this feature by setting the
266 bathymetry of the convergent part as:

$$267 \quad H(x, y) = H_{min} + (H_m - H_{min})\frac{y}{L} + (H_{max} - H_{min}) \times \left(1 - \frac{y}{L}\right) \left(1 - \frac{4x^2}{B^2}\right) e^{-C_f \left(\frac{4x^2}{B^2}\right)} \quad (2)$$

268 where L is the length of the convergent part (70 km); H_{max} (20 m) and H_{min} (3.0 m)
269 are the maximum and minimum water depths at the estuary mouth, the width-averaged
270 water depth H_m is constant ($H_m=8$ m) along the estuary, and the parameter C_f is set
271 as 4, based on the bathymetry data. In the straight part of the estuary, the bathymetry
272 was kept the same as that of the uppermost cross-section of the convergent part.

273 At a distance of 75 km from the mouth of the main estuary, we added a sub-estuary
274 on the east side, resembling the East River sub-estuary. The sub-estuary extends in a
275 southwest-northeast direction for a distance of approximately 75 km. The width of the
276 sub-estuary is ~~mildly~~ convergent, with a width of 10 km at the confluence and
277 decreasing to 600 m at the head, with an e-folding decrease scale (L_b) of ~~90~~26.7 km.
278 The water depth decreases landward from 6 m at the confluence to 3.5 m at the head of
279 the sub-estuary.

280 As the boundary conditions at an estuary mouth are generally unknown, we added
281 a continental shelf to the model domain. The shelf is 100 km wide and approximately
282 500 km long, with the downstream part (representing the Kelvin wave propagation
283 direction) being slightly longer than the upstream part. The water depth of the shelf is
284 uniform in the alongshore direction and increases linearly from the coast to the offshore
285 direction, with a slope of 1×10^{-4} . The model grid has 313×506 cells, with a cross-
286 channel spatial resolution of 300 m and an along-channel resolution of 500 m in the

287 estuary. The horizontal resolution decreases on the shelf and becomes 2 km at the open
288 ocean boundaries. Fifteen vertical s-grid layers were specified with higher resolutions
289 near the surface and bottom, and the coefficients of θ_s , θ_b , and h_c were set as 2.5,
290 3.0, and 5.0, respectively. In ROMS Model, coefficients larger than unity for θ_s , θ_b
291 can generate higher resolutions near the surface and bottom, respectively. For details of
292 these coefficients, ~~the reference of~~ Shchepetkin and McWilliams (2005) can be referred
293 to.

294 We used the $k - \varepsilon$ submodel of the Generic Length Scale (*GLS*) turbulence
295 closure scheme to calculate the vertical mixing (Umlauf and Burchard, 2003; Warner
296 et al., 2005). The horizontal eddy viscosity and diffusivity were calculated using the
297 Smagorinsky scheme (Smagorinsky, 1963). The bottom friction was calculated based
298 on the log-layer assumption near the bottom, with a bottom roughness length of 1 mm.
299 This setting results in a mean bottom drag coefficient of 0.005. The open ocean
300 boundary condition for the barotropic component consists of a Flather/Chapman
301 boundary condition for the depth-averaged flow and sea surface elevation (Chapman,
302 1985; Flather, 1976). The open boundary conditions for the temperature, salinity, and
303 baroclinic current are the Orlanski-type radiation conditions (Orlanski, 1976).

304 To investigate the impact of salt dynamics in the main estuary on salt intrusion in
305 the sub-estuary, two numerical experiments were implemented. In both cases, the river
306 discharge at the head of the sub-estuary was set as 200 m³/s, which is approximately
307 the value during the dry season in 2021 in the East River estuary. A time series of water
308 levels produced by a combination of 12 tidal constituents was specified at the offshore
309 boundary. These 12 tidal constituents are M_2 , S_2 , N_2 , K_2 , K_1 ,
310 O_1 , P_1 , Q_1 , M_4 , MS_4 , M_m , M_f , respectively. The tidal constants of these 12

311 constituents were obtained from the Oregon Tidal Database (OPTS). As the tidal
 312 amplitudes are almost doubled at the mouth of the main estuary due to the
 313 superimposition of propagating and reflected tidal waves, the amplitudes of these tidal
 314 constituents at the offshore boundary were reduced by half. Case 1 was set with a river
 315 discharge of $1,500 \text{ m}^3 \text{ s}^{-1}$ at the main estuary's head. The river discharge of $1500 \text{ m}^3 / \text{s}$
 316 is representative of the total amount that empties into the PRE from different outlets in
 317 dry seasons (Gong et al., 2020), being lumped as input at the head of the PRE. The
 318 inflowing river water was prescribed to have zero salinity and a temperature of 22°C ,
 319 identical to the background temperature setting throughout the entire domain. The
 320 incoming salinity at the offshore boundary was specified to be 34 psu ~~psu~~ kgg/kg. In Case
 321 2, we set an extremely low river discharge ($500 \text{ m}^3 \text{ s}^{-1}$) at the head of the main estuary,
 322 which is realistic under the La Nina event. In this scenario, we aimed to check how the
 323 salt dynamics in the more mixed main estuary affect the salinity variation in the sub-
 324 estuary.

325

326 3.3 Analytical solutions for the salinity variation in the well-mixed sub-estuary

327

328 For the ~~subtidal (here is that averaged over 25 hours)~~ tidally-averaged salinity
 329 variation along the well-mixed sub-estuary, the advection-diffusion equation can be
 330 written as:

$$331 \quad \frac{\partial(A\bar{S})}{\partial t} = -\frac{\partial}{\partial x}(A\bar{u}\bar{S}) + \frac{\partial}{\partial x}(AK_x \frac{\partial \bar{S}}{\partial x}) \quad (3)$$

332 where A is the cross-sectional area, \bar{S} is the ~~subtidal~~ tidally-averaged salinity in the
 333 cross-section, t is time, \bar{u} is ~~subtidal~~ tidally-averaged longitudinal velocity, x is the

334 distance along the sub-estuary, K_x is the longitudinal dispersion coefficient. The left
 335 term in Eq. 3 indicates the local acceleration and the unsteadiness of salinity variation.
 336 The unsteadiness is controlled by the contrast between the internal and external
 337 timescales. ~~The internal timescale of the sub-estuary for a river discharge of 200 m³/s~~
 338 ~~was estimated to be longer than 30 days. This timescale is longer than the fortnightly~~
 339 ~~timescale, and the salinity in the sub-estuary can hardly reach a steady state under the~~
 340 ~~varying tides, thus the time tendency term should not be ignored.~~ Savenije (2012)
 341 suggested another an internal timescale to quantify the sub-estuary's response timescale
 342 (T_S), which is expressed as:

$$343 \quad T_S = -\frac{1}{Q_f \bar{S}(X)} \int_X^L A \bar{S} dx \quad (4)$$

344 Based on the numerical model results, by selecting X at the sub-estuary's mouth,
 345 we calculated the response timescale to be 16.22 day, which is comparable to the spring-
 346 neap tidal cycle. This indicates that the salinity ~~variation~~ in the sub-estuary can
 347 approximately keep pace vary along with the changing tidal forcing. We thus ignored
 348 the unsteadiness term and assumed that the horizontal dispersion is constant in a
 349 ~~subtidal-tidal~~ period and scales with the tidal current at the sub-estuary's mouth.
 350 Meanwhile, the boundary condition of ~~subtidal-tidally-averaged~~ salinity at the sub-
 351 estuary's mouth was updated at each ~~subtidal-tidal~~ period. In this way, the calculation
 352 of ~~subtidal-tidally-averaged~~ salinity in the sub-estuary can ~~be proceeded~~ proceed. As
 353 such, Eq. 3 becomes (Cai et al., 2015):

$$354 \quad \frac{Q}{A} \bar{S} = K_x \frac{\partial \bar{S}}{\partial x} \quad (5)$$

355 in which Q is the river discharge. We assume that the cross-sectional area decreases

356 exponentially in the landward, $A = A_0 \exp(-x/a)$, where a is the convergence
 357 length scale of the cross-sectional area. When the longitudinal dispersion coefficient
 358 K_x is assumed to be a constant along the sub-estuary, the ~~subtidal-tidally-averaged~~
 359 salinity along the sub-estuary can be obtained as:

$$360 \quad \frac{\bar{S}}{S_0} = \exp\left\{-\frac{Qa}{A_0 K_x} \left[\exp\left(\frac{x}{a}\right) - 1\right]\right\} \quad (6)$$

361 For each ~~subtidal-tidal~~ period, we obtained the ~~tidally-averagedsubtidal~~ salinity
 362 (S_0) and the tidal current at the mouth of the sub-estuary from the numerical model
 363 results, and related the horizontal dispersion (K_x) to the tidal strength at the mouth.
 364 When these data were available, the ~~tidally-averagedsubtidal~~ salinity at each ~~subtidal~~
 365 ~~tidal~~ period was calculated for our numerical simulation period.

366 When the K_x is assumed to vary along the estuary, the salinity variation along the
 367 sub-estuary is in another form and not presented here (Savenije, 2012), as that form of
 368 K_x is not related to the tidal strength and is unsuitable for our situation here, so this
 369 scenario is not pursued further.

370

371 **3.4 Calculation of the salt and freshwater fluxes**

372

373 The salt flux at a cross-section is calculated as follows:

$$374 \quad F_s = \int u S dA \quad (7)$$

375 where u is the instantaneous longitudinal velocity, and S is the instantaneous
 376 salinity. The instantaneous flux was integrated and then averaged over a ~~subtidal~~
 377 ~~period-(25 hours).~~

378 As the changes in freshwater transport by the river-tide interaction are concerned,
 379 we also calculated the freshwater flux, which is:

$$380 \quad F_f = \int u \left(1 - \frac{S}{S_0}\right) dA \quad (8)$$

381 where S_0 is the ocean salinity, here is taken to be 34 ~~psu/kg/kg~~. The freshwater flux
382 was also integrated and averaged over ~~a tidal period~~ a subtidal timescale.

383

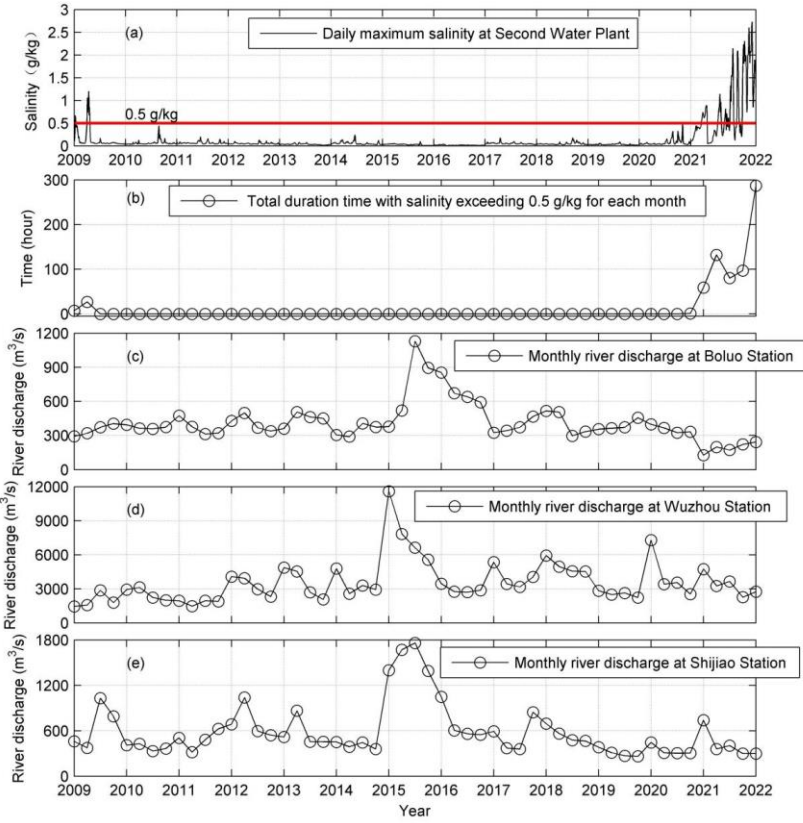
384 **4. Results**

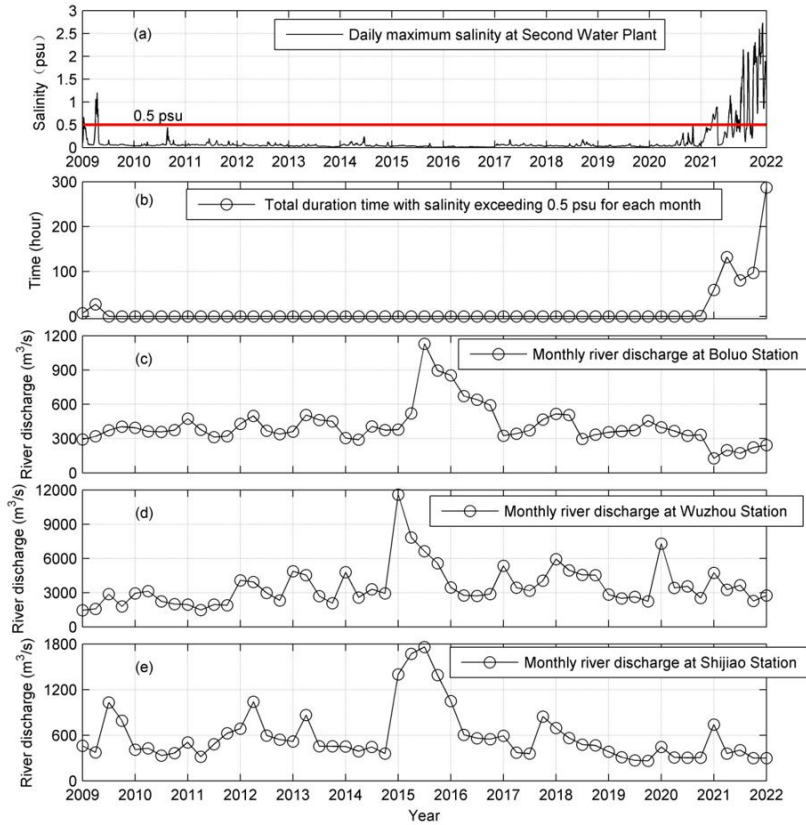
385

386 **4.1 The characteristics of salt dynamics in the sub-estuary: based on observation** 387 **data**

388

389 Here we take the Second Water Plant as a representative station in the upstream
390 region of the sub-estuary. The salinity variation at this station was checked from 2009
391 to 2022, as shown in Fig. 3. It indicates (Fig. 3a) that before 2021, the surface salinity
392 was generally lower than 0.5 ~~psu/kg/kg~~ and suitable for extraction. During the winter
393 season of 2021-2022, the salinity exceeded the drinking water criterion for a prolonged
394 period of 280 hours in January 2022 (Fig. 3b). These elevated salinities coincided with
395 the decreased river discharge from the upstream in the PRD, shown by the data at the
396 hydrological stations of Boluo, Wuzhou and Shijiao (Figs. 3c, 3d and 3e). Note that the
397 river discharges in 2022 are comparable to those of 2009, but the effect on salinities are
398 dramatically higher. The reasons behind such a difference is not clear right now, but
399 could be due to the increased water depth along the sub-estuary in 2022 by sand mining,
400 and/or the elevated water level outside the sub-estuary due to wind effects.—

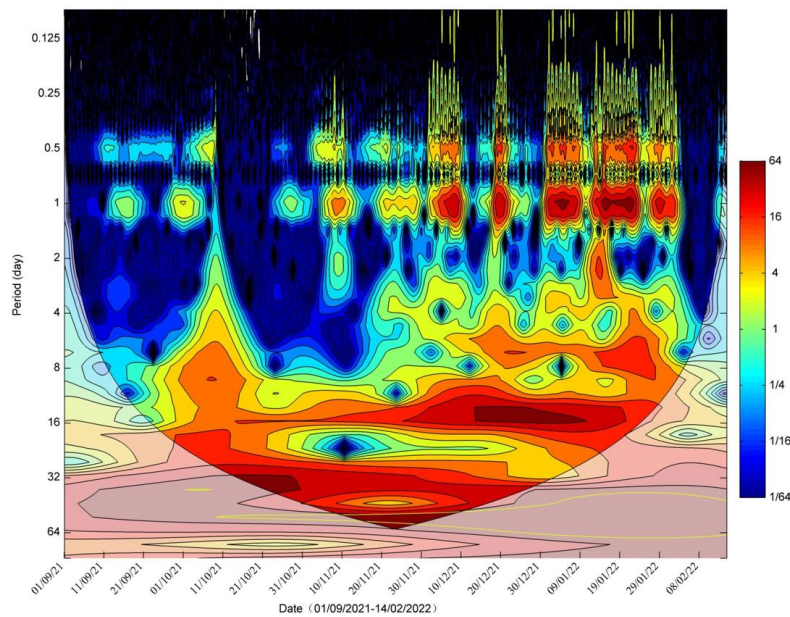




402
 403 Fig.3. Timeseries of: a) Daily maximum salinity at the Second Water Plant; b) Total duration period
 404 with salinity exceeding 0.5 ~~psu/kg~~ for each month; c) Monthly river discharge at Boluo station
 405 (upstream of the East River); d) Monthly river discharge at Wuzhou station (upstream of the West
 406 River); e) Monthly river discharge at Shijiao station (upstream of the North River). ~~Note that the~~
 407 ~~river discharges in 2022 are comparable to those of 2009 but the effect on salinities are dramatically~~
 408 ~~higher.~~

409
 410 We conducted wavelet analysis for the salinity data of the Second Water Plant
 411 Station from September 2021 to February 2022, when the salt intrusion was severe. The

412 result is shown in Fig. 4. It indicates that the power of salinity variations is concentrated
413 in several periods: one is in the range of 0.5 to 1 day, which is caused by tidal fluctuation;
414 the second period lies in the range of 5-9 days, which is presumably induced by wind
415 forcing; the third one is in the range of 14-16 days, obviously by the fortnightly
416 variation of spring-neap tidal cycle. The last one is within the range of 28 days, near
417 the monthly timescale. This periodicity should be caused by the tidal beating among
418 tidal constituents of M_2 , S_2 , N_2 , K_1 , O_1 , as indicated by Payo-Payo et al. (2022).

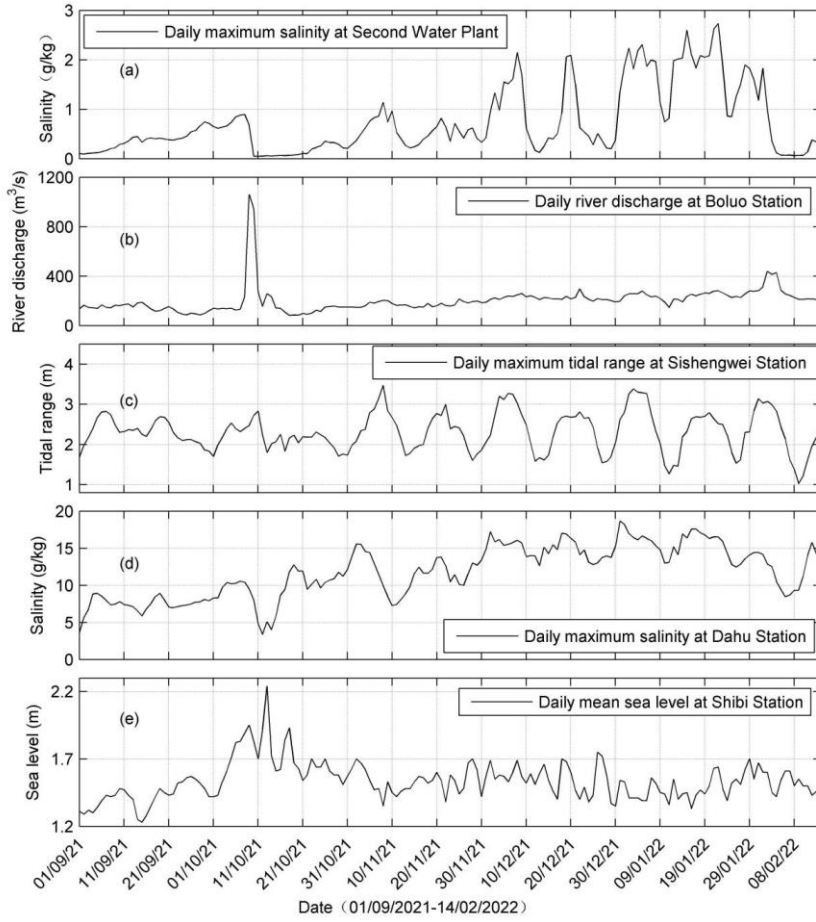


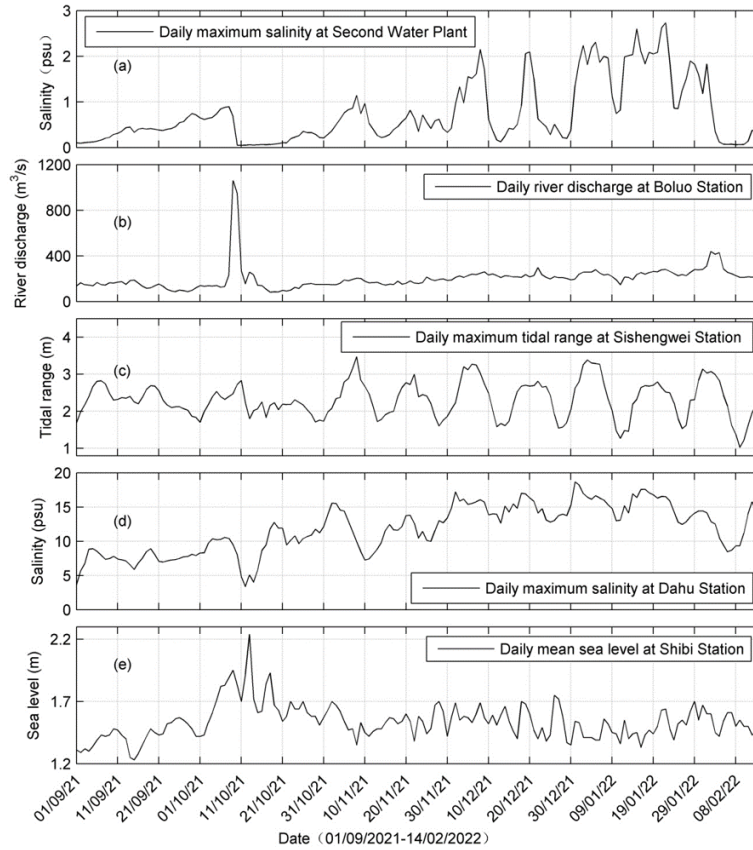
419
420 Fig. 4 Wavelet analysis of the salinity at the Second Water Plant

421
422 To identify the possible factors influencing the salinity variations in the sub-
423 estuary, we present the time series data of salinity at the Second Water Plant, river
424 discharge at Boluo station, tidal range at Sishengwei station, salinity at Dahu station

425 (located in the main estuary), and daily sea level at Shibi station (located at the mouth
426 of the main estuary) in Fig. 5. Firstly, it is evident that the variation of salinity at Dahu
427 (Fig. 5d) shows a consistent pattern with the changes in tidal range at Sishengwei (Fig.
428 5c), when the river discharge is relatively low after a flash flood event, which occurred
429 around October 21, 2021 (Fig. 5b). The highest salinity happened 2-3 days after neap
430 tides in the transition from neap to spring tides, whereas the lowest salinity occurred in
431 the transition from spring to neap tides, and generally occurred just before the neap
432 tides. This result indicates that the salinity and tidal range in the main estuary were
433 almost out of phase, and there existed a time lead of the salinity to the tidal range. This
434 pattern agrees well with what occurred in the Hudson River (Bowen and Geyer, 2003)
435 and the Modaomen Estuary (Gong and Shen, 2011), suggesting that the PRE remained
436 in a state of partially mixed. On the other hand, the salinity of the Second Water Plant
437 was almost in phase with the tidal range at the confluence (Fig. 5a vs. 5c). High
438 salinities coincided with spring tides, and low salinities occurred during neap tides. It
439 should be noted that the sea level at the PRE mouth showed a significant setup near
440 October 11, 2021, when a large increase in river discharge was observed in the PRD
441 due to a tropical storm (enumerated as the 17th typhoon in 2021, see the peak in Fig.
442 5b). This event caused a sharp decline in salinities at both Dahu and the Second Water
443 Plant, followed by a rebound approximately 10 days later. Note that it takes about 7-8
444 days after the storm for the salinity to recover to its pre-storm levels in the main estuary
445 and almost a month in the sub-estuary. The recovery time is mostly determined by the
446 landward salt flux, as pointed out by Du and Park (2019). The landward salt flux is larger

447 in the main estuary as it is more stratified and the estuarine circulation is more developed,
448 which generate a larger steady shear transport. Meanwhile the width and the cross-sectional
449 area of the main estuary are larger, favorable for the salt import from the ocean. Moreover,
450 the station at the main estuary is located downstream of the confluence between the main
451 estuary and the sub-estuary. After the salinity recovery at the station in the main estuary,
452 the elevated salinity then propagates from the confluence to the upstream of the sub-estuary,
453 where the station at the sub-estuary is located. As the cross-section at the confluence is
454 small, the landward salt flux is limited, further increasing the recovery time for the station
455 at the sub-estuary.





457

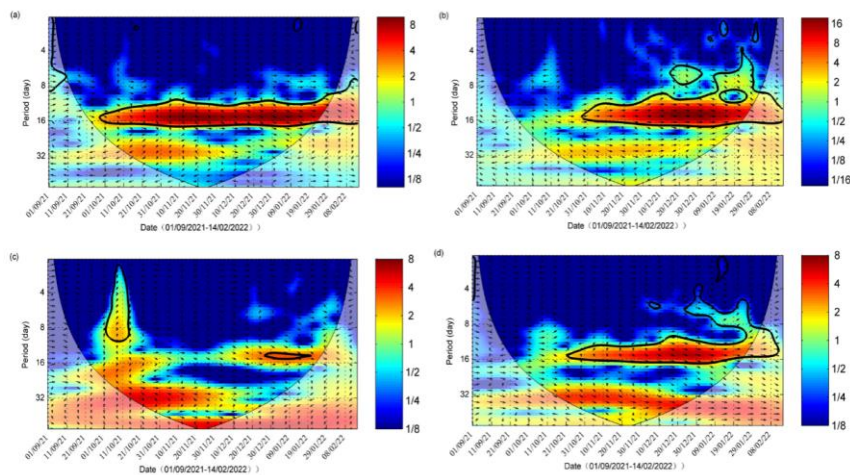
458 Fig. 5. Timeseries of: a) Daily maximum salinity at the Second Water Plant; b) Daily river
 459 discharge at Boluo station; c) Daily maximum tidal range at Sishengwei Station; d) Daily

460 maximum salinity at Dahu Station; e) Daily mean sea level at Shibi Station. ~~Note that it takes~~
 461 ~~about 7-8 days after the storm for the salinity to recover to its pre-storm levels in the main estuary~~
 462 ~~and almost a month in the sub-estuary~~

463

464 The cross-wavelet analysis between salinity at Dahu and tidal range at Sishengwei
 465 (Figs. 6a) shows that the two variables are highly correlated in the periods of 14-16
 466 days, indicating the effect of fortnightly spring-neap tidal variation. The arrow pointing

467 down and right in this time band demonstrates that the change in tidal range lagged the
468 variation of salinity.



469
470 Fig. 6. Cross-wavelet analysis of (a) between the salinity at Dahu and the tidal range at
471 Sishengwei; (b) between the salinity at the Second Water Plant and the tidal range at Sishengwei;
472 (c) between the salinity at the Second Water plant and the river discharge at the Boluo Station; (d)
473 between the salinity at the Second Water plant and that at the Dahu Station.

474
475 The cross-wavelet analysis between the salinity at the Second Water Plant and the
476 tidal range at Sishengwei station (Figs. 6b) shows that there existed a high common
477 power band of 14-16 days after October 21, 2021, and the phase relationship between
478 them was in phase, indicating that high salinities occurred during spring tides and low
479 salinities during neap tides, confirming the above results. It is also noted that before the
480 flood event on October 11, 2021, there was no high common power between these two
481 variables, even though the river discharge at the head of East River (Boluo Station) was

482 lower. This lack of high common power in the time band of 14-16 days before the
483 tropical storm event can also be noted in the cross-wavelet analysis between the salinity
484 at Dahu and the tidal range at Sishengwei. We also noted that before the storm event,
485 the water level at Sishengwei did not show distinct fortnightly spring-neap variations
486 (Fig. 5c). This lack of fortnightly cycle could be induced by the wind-induced
487 setup/setdown and/or the river-tide interaction, in which the river flow suppress the
488 tidal propagation. This phenomenon is peculiar and warrants a future study but beyond
489 the scope of this study.

490 The cross-wavelet analysis between the salinity at the Second Water Plant and the
491 river discharge at Boluo Station is presented in Fig. 6c. The high correlation during the
492 storm event was obvious, whereas, after that, the common power between the salinity
493 and river discharge was relatively low during the rebound period of the salinity at the
494 Second Water Plant. This low correlation could be due to the fact that the river discharge
495 did not change much and had no periodicity of 14-16 days then.

496 To examine the relationship between the salinities in the main estuary and at the
497 sub-estuary, we conducted a cross-wavelet analysis between the salinity at the Second
498 Water Plant and that at Dahu (Fig. 6d). There existed high common power between
499 these two variables in the time band of 14-16 days, the fortnightly tidal cycle. It also
500 shows that before October 21, 2021, the phase relationship between these two variables
501 was approximately in quadrature, indicating that the variation of the salinity at the
502 Second Water Plant lagged that at Dahu by 3.5-4 days. After October 21, 2021, the
503 phase relationship between them changed to in-phase when the river discharges in the

504 PRD became very low. This is quite interesting and will be explored in the following.

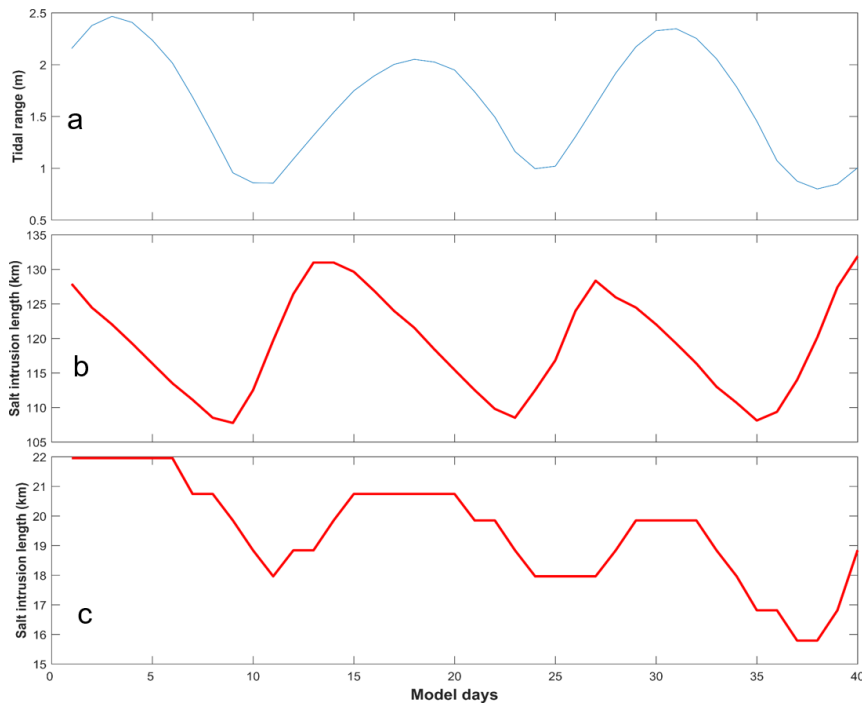
505

506 **4.2 The salt dynamics obtained through numerical simulations**

507

508 For Case 1 (base run), we intended to investigate the salt dynamics when the main
509 estuary stays in a state of partially mixed. Firstly we examine the variation of salt
510 intrusion length along the estuary's deep channel (Fig. 2b). Here the salt intrusion
511 length is defined as the distance of the bottom salinity isohaline of 5 ~~psu~~kg/kg from
512 the estuary mouth. It shows that the tidal range at the main estuary's mouth fluctuates
513 at fortnightly and monthly timescales. There occur two spring tides and neap tides in a
514 month (Fig. 7a), with one spring (neap) tide being stronger than the other one, as the
515 perigee/apogee cycle. The salt intrusion in the main estuary fluctuates with the tidal
516 range (Fig. 7b). The maximum salt intrusions occur just after neap tides, and the
517 minimum salt intrusions occur at the late of the transition from spring to neap tides,
518 consistent with the salinity change at the Dahu station shown above (Fig. 5d), and the
519 results we have demonstrated before (Gong et al., 2018). The relationship between the
520 salt intrusion and tidal range indicates an almost anti-phase one, suggesting that the
521 estuary is basically in a state of partially-mixed. This is because, for a partially-mixed
522 estuary, the landward salt transport is maximum during neap tides by the steady shear
523 and results in a maximum salt intrusion then. We present the tidally averaged
524 longitudinal profile of current and salinity for representative neap and spring tides in
525 Fig. S1 in the Supplement. The results confirm that during the neap tide, the estuary is
526 partially mixed, whereas, during the spring tide, the estuary becomes more mixed but

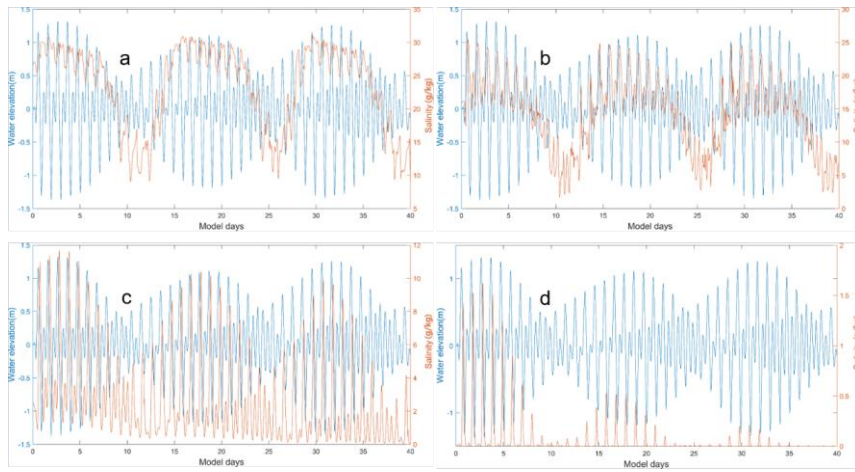
527 still in the state of partially mixed.



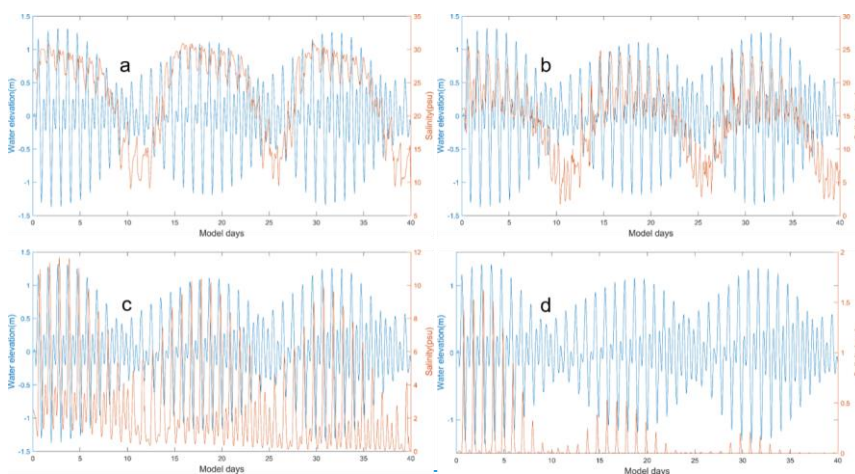
528
529 Fig. 7. Timeseries of: a) tidal range at the mouth of the main estuary; b) salt intrusion length along
530 the longitudinal section of the main estuary; c) salt intrusion length along the longitudinal section
531 of the sub-estuary.

532
533 We also checked the time series data of surface salinity and water level at a station
534 (S1, Fig. 2b) in the main estuary, roughly corresponding to the Dahu Station (Fig. 8a).
535 It shows that the surface salinity increases from neap to spring tides, and reaches
536 maxima before spring tides. It declines from the maxima to minima from spring to neap
537 tides, reaching the minima almost at neap tides. This shows that the salinity increases
538 faster from neap to spring than decreases from spring to neap. This asymmetry is also

539 noted in the variation of salt intrusion length, which increases sharply after the neap
540 tides but decreases more gradually from the maximum to the minimum. This
541 phenomenon has been discussed by Chen (2015); when the salt intrusion length is
542 shorter just before the neap tide, the acceleration by the net landward salt flux is stronger,
543 whereas when the salt intrusion length is longer, the deceleration of salt intrusion length
544 by net seaward salt flux is relatively weaker. The change in salinity leads that in tidal
545 range during spring tides but lags the tidal range during neap tides.



546



547

548 Fig. 8. Timeseries of water level at the confluence and surface salinity a) at S1 Station in the main
549 estuary; b) at S2 station (the confluence); c) at S3 station in the middle of the sub-estuary; d) at S4
550 station in the upstream region of the sub-estuary.

551

552 Similar to the analysis of observation data, we then investigate the salt intrusion
553 in the sub-estuary (Fig. 7c). Though the accuracy is not high, as our model resolution
554 in the sub-estuary is not fine enough, it clearly shows that the maximum salt intrusions
555 occur nearly in spring tides and the minimum salt intrusions in neap tides. This means
556 that the salt intrusion is in phase with the tidal range in the sub-estuary. We show the
557 tidally averaged profiles of current and salinity at the sub-estuary in Fig. S2 in the
558 Supplement. It indicates that the sub-estuary is mostly in a state of well-mixed during
559 both the neap and spring tides, though there appears some stratification near the mouth
560 of the sub-estuary during the neap tide. The 1 psu/kg/kg isohaline intrudes more in
561 spring tides than in neap tides. It should be noted that at the lower reach of the sub-
562 estuary, the surface salinity has a local high salinity zone (Fig. S2), consistent with the
563 finding of Haywood et al. (1982) at the lower York River in the Chesapeake Bay, USA.

564 To examine the salinity variations along the sub-estuary, we selected three stations
565 in the sub-estuary: one at the mouth (S2), one in the middle reach (S3), and the last one
566 in the upper reach (S4). The time series of water level at the confluence and salinities
567 at these three stations are shown in Figs. 8b, 8c and 8d. The salinity at the mouth of the
568 sub-estuary (Fig. 8b) fluctuates similarly to that in the main estuary: maximum salinities
569 occur right after neap tides and minimum salinities just before neap tides. In the middle

570 of the sub-estuary (Fig. 8c), the salinity variation almost keeps pace with that of the
571 tidal range: maximum salinities occur at spring tides and minimum salinities at neap
572 tides. At the upstream station, the salinity variation shows a similar pattern to that in
573 the middle of the sub-estuary. This indicates that when saline water propagates
574 upstream, it advances more landward and experiences less impedance during spring
575 tides and vice versa. We explore this phenomenon in the discussion part.

576

577 **4.3 The ~~subtidal~~tidally-averaged salt dynamics in the sub-estuary by the analytical** 578 **solution**

579

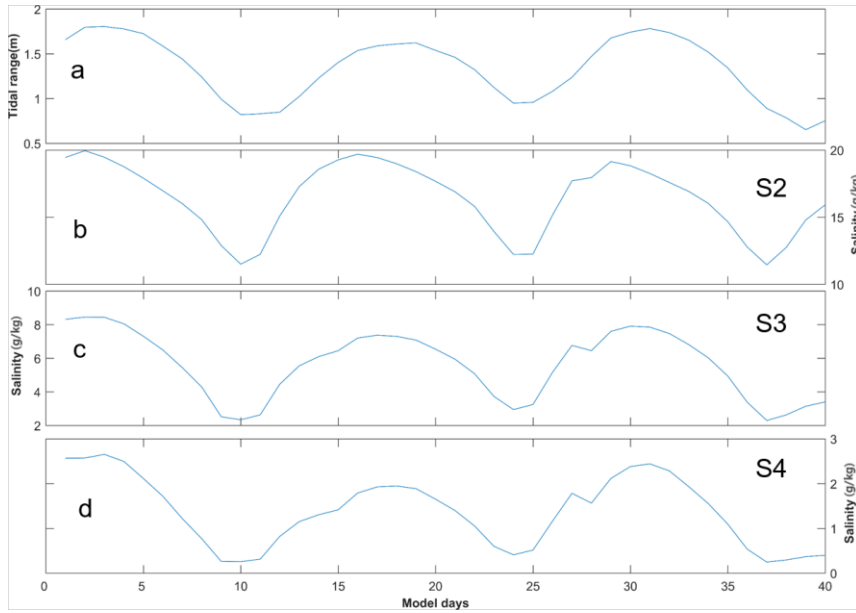
580 We used the analytical solutions in Section 3.3 to explore the salt dynamics in the
581 sub-estuary. In the sub-estuary, the exponential decaying constant of the cross-sectional
582 area was calculated to be 50 km; and the river discharge was specified to be 200 m³ s⁻
583 ¹.

584 We used the scheme of constant dispersion along the sub-estuary, and the K_x was
585 estimated as (Ralston et al., 2008):

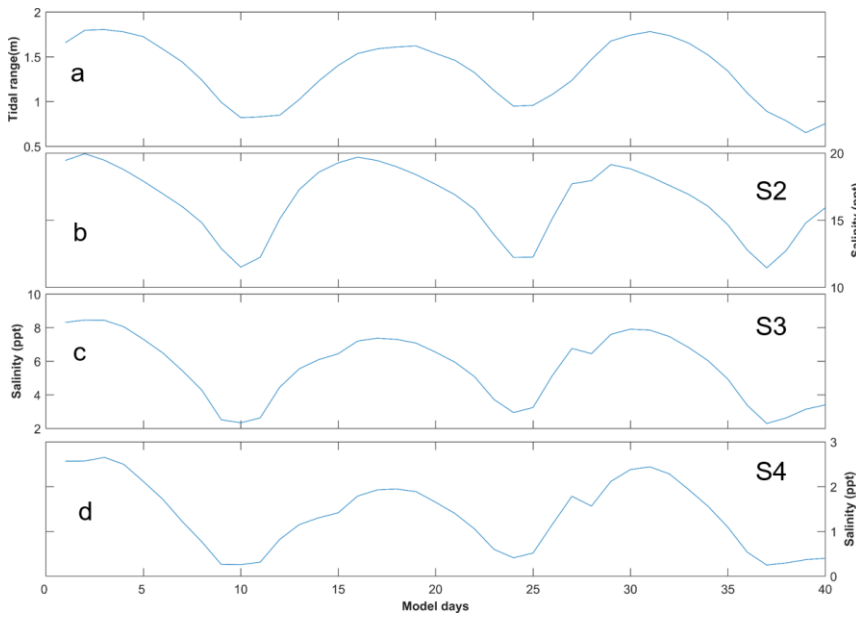
$$586 \quad K_x = c_h \left(\frac{T_{tide}}{4} U_T \right) U_T \quad (9)$$

587 where c_h is an empirical constant of 0.0224, T_{tide} is the tidal period, here is set as
588 12.42 hours; U_T is the tidal current amplitude at the sub-estuary's mouth.

589 We solved Eq. (6) for the model experiment Case 1. The results are shown in Fig.
590 9.



591



592

593

594

595

Fig. 9. The results of the analytical solution of salinity variations along the sub-estuary. a) tidal range at the mouth of the sub-estuary; b), c), and d) are tidally-averaged salinity variations at S2, S3, and S4 stations.

带格式的: 默认段落字体, 字体: 等线, 五号

596

597 Under the $1500 \text{ m}^3 \text{ s}^{-1}$ river discharge at the head of the main estuary, the tidal
598 range at the sub-estuary's mouth varies between spring and neap tides, with a greater
599 spring and a weaker spring in a month (Fig. 9a). The tidally-averaged subtidal salinity
600 at the confluence (S2 station, Fig. 9b) varies between 10 and 20 $\text{psu} \text{ kg/kg}$, with the
601 maximum salinities occurring before the spring tides and the minimum salinities before
602 the neap tides, indicating a phase lead of salinity to the tidal range. In the middle of the
603 sub-estuary (S3 station, Fig. 9c), the salinity fluctuates between 2 and 10 $\text{psu} \text{ kg/kg}$,
604 and there exists a slight phase lead of salinity to that of the tidal range. In the upstream
605 region of the sub-estuary (S4 station, Fig. 9d), the salinity fluctuates between 0 and 3
606 $\text{psu} \text{ kg/kg}$, and the salinity variation becomes almost in phase with that of the tidal
607 range at the confluence. Compared to the numerical simulation results, the analytical
608 solution reproduces the trend of the phase relationship between the salinity and tidal
609 range along the sub-estuary: the phase of the salinity variation leads that of the tidal
610 range at the sub-estuary's mouth and becomes more in phase with that of the tidal range
611 in the middle and upstream region of the sub-estuary. Meanwhile, the fluctuation
612 magnitude in the middle of the sub-estuary is well reproduced. However, the fluctuation
613 range in the upstream region of the sub-estuary is over-estimated, showing the
614 weakness of assuming a uniform horizontal dispersion along the sub-estuary.

615

616 5. Discussion

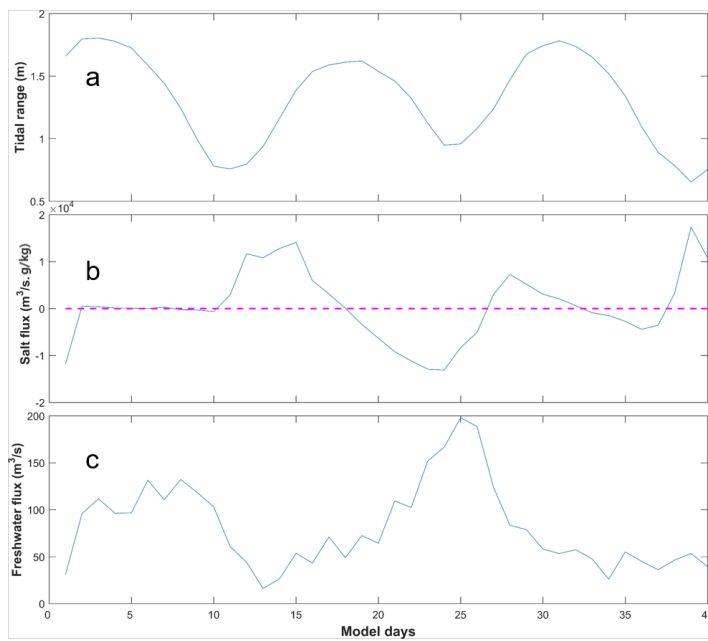
617

618 5.1 The physics behind the change in phase relationship between the salinity and 619 tidal range along the sub-estuary

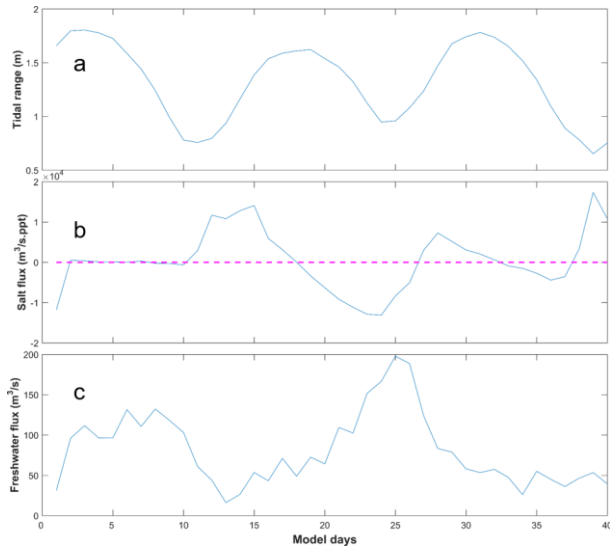
620

621 The numerical results and analytical solutions both indicate that near the sub-
622 estuary's mouth, the salinity fluctuation leads that of the tidal range, and in the middle
623 and upstream region of the sub-estuary, the salinity variation becomes more in phase

624 with that of the tidal range. The analytical solution shows that the changes in the phase
625 relationship between these two variables are mostly caused by the change in horizontal
626 dispersion, that is, the larger dispersions during spring tides cause increased landward
627 salt transport, resulting in elevated salinity in the middle and upstream regions of the
628 sub-estuary. The results of numerical simulation are a combination of many
629 interweaved processes and a little harder to interpret. To unravel the physics in the
630 numerical simulation, we examine the salt transport in the lower reach at a cross-section
631 near the sub-estuary mouth and freshwater transport in the upstream cross-section of
632 the sub-estuary (shown in Fig. 2b).



633



634
635
636

637 Fig. 10. Timeseries of: a) tidal range at the mouth of the sub-estuary; b) salt flux at the
638 cross-section near the mouth of the sub-estuary; c) freshwater flux at the cross-section in the
639 upstream region of the sub-estuary. It should be noted that the freshwater flux is the magnitude
640 and has a sign opposite to the salt flux.

641

642 The results are shown in Fig. 10. From Fig. 10b, the ~~tidally-averagedsubtidal~~ salt
643 flux near the sub-estuary's mouth is generally landward during the periods from neap
644 tides to spring tides and seaward from spring tides to neap tides. The change in salt flux
645 leads that of the tidal range, consistent with the phase relationship between salinity and
646 tidal range near the sub-estuary's mouth (Fig. 8b). As the sub-estuary is well-mixed
647 during the simulation period, the landward salt transport is mostly induced by the tidal
648 oscillatory transport. The ~~tidally-averagedsubtidal~~ freshwater flux in the upstream

649 region of the sub-estuary is seaward, and shows a pattern that larger freshwater fluxes
650 occur during neap tides and smaller freshwater fluxes during spring tides (Fig. 10c).
651 This pattern has been well studied by Buschman et al. (2009) in the tidally-
652 averagedsubtidal momentum dynamics. They showed that the primary tidally-
653 averagedsubtidal momentum balance is between the water level gradient and bottom
654 friction. During spring tides, the tidally-averagedsubtidal bottom friction is larger and
655 the subtidal-tidally-averaged water slope is greater, meaning that more freshwater is
656 being detained upstream to elevate the water level there. During neap tides, the detained
657 freshwater in the upstream is released downstream and results in increased freshwater
658 fluxes. In this way, the saline water from the sub-estuary's mouth experiences less
659 impedance and dilution during spring tides and thus advances more landward, resulting
660 in an enhanced salt intrusion during spring tides, and vice versa. The above results
661 indicate that the more in-phase relationship between the salinity and tidal range in the
662 middle and upstream region of the sub-estuary is mostly generated by the fortnightly
663 variation of the tidal strength and the associated variations of horizontal dispersion and
664 freshwater flux by the river-tide interaction. The larger the dispersion, the more salt is
665 pumped into the upstream. The stronger the tidal strength, the more freshwater is
666 detained upstream and less impedance to the salt intrusion.

667 From the above results, it is seen that the salinity dynamics in the sub-estuary show
668 a pattern that is more influenced by the main estuary in the lower reach and becomes
669 more controlled by internal tidal processes in the middle and upstream regions of the
670 sub-estuary.

671

672 **5.2 How do the salt dynamics in the main estuary affect that in the sub-estuary?**

673

674 To further study how the changes in salinity dynamics in the main estuary affect

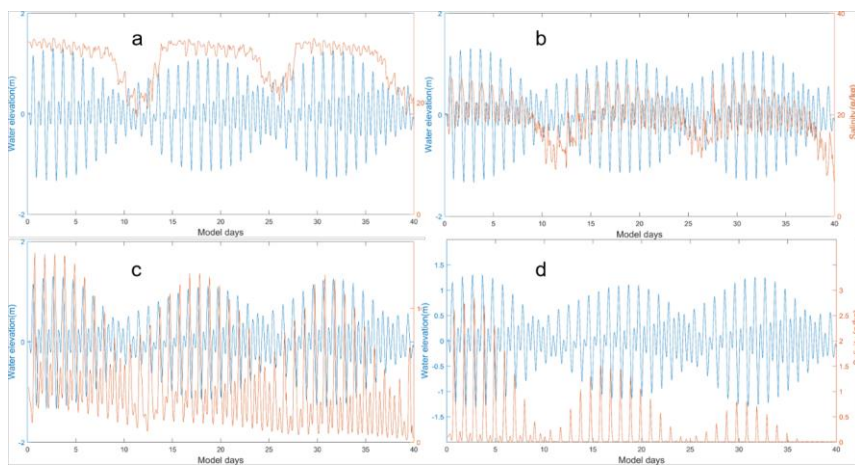
675 the salinity variation in the sub-estuary, we set up another experiment. In the model

676 scenario of Case 2, we set an extremely low river discharge ($500 \text{ m}^3 \text{ s}^{-1}$) at the head of

677 the main estuary, and the results are shown in Fig. 11. Simultaneously, the analytical

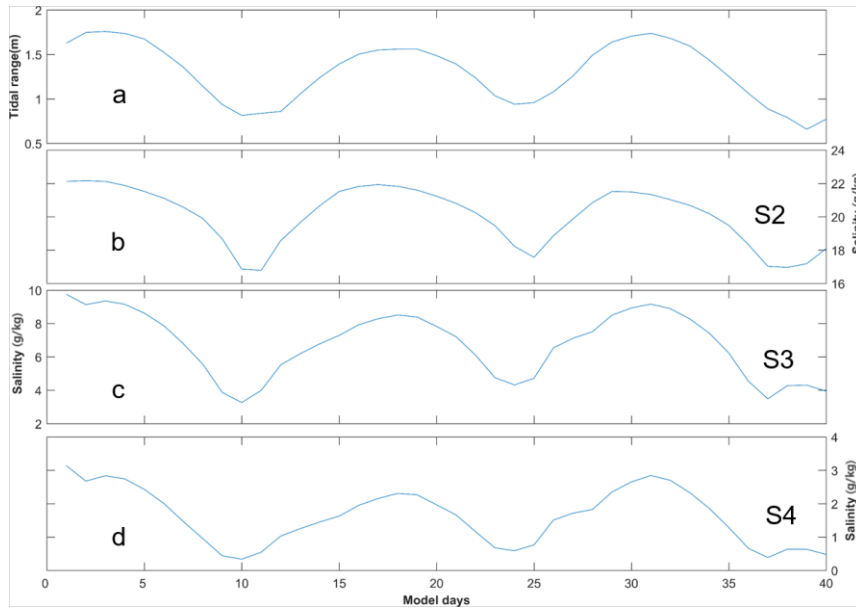
678 solutions for the scenario of Case 2 are presented in Fig. 12.

679

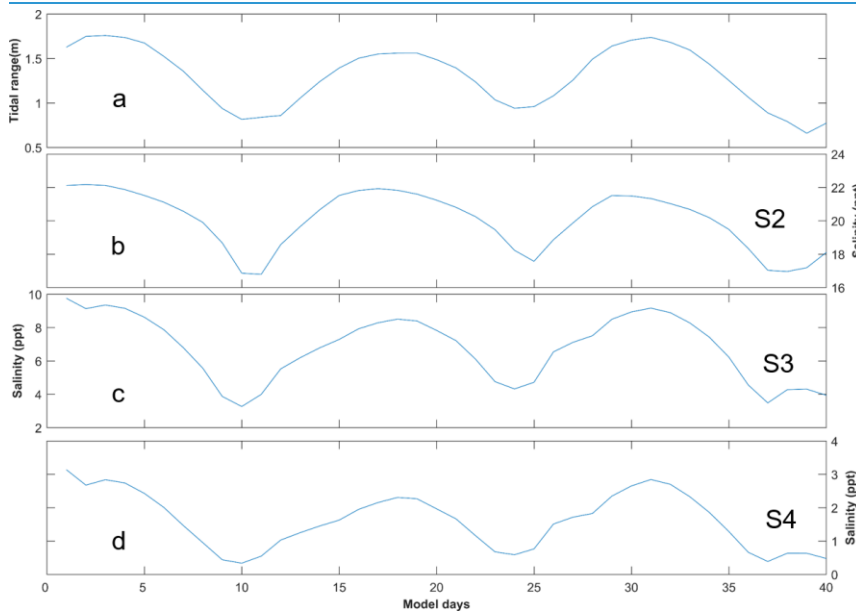


680

681 Fig. 11. Timeseries of water level at the confluence and surface salinity under the
682 extremely lower river discharge in the main estuary at stations of: a) S1; b) S2; c) S3; d) S4.
683



684



685

686 Fig. 12. The results of the analytical solution of salinity variations along the sub-estuary
687 under extremely dry conditions. a) tidal range at the mouth of the sub-estuary; b), c), and d) are
688 tidally-averaged~~subtidal~~ salinity variations at S2, S3, and S4 stations.

689
690 With decreased river discharge from the head of the main estuary, the salt intrusion
691 front is shifted more landward. The S1 station is now located in the polyhaline region
692 with a mean salinity of approximately 26 ~~psu~~psu/kg/kg (Fig. 11a). The minimum
693 salinities coincide more with neap tides but the maximum salinities occur around spring
694 tides. The asymmetry between salinity rise and fall is decreased, with salinities jumping
695 quickly after neap tides, keeping elevated around spring tides, and dropping quickly
696 just before neap tides. For the intratidal variation, it can be seen that during a tidal cycle,
697 the salinity fluctuation is reduced when compared to Case 1 (Figs. 11a vs 8a), which is
698 mostly due to the fact that with the reduced river discharge, the salinity gradient in the
699 polyhaline reach of the main estuary is decreased.

700 For the S2 Station (at the confluence, Figs. 11b and 12b), it is now located in the
701 mesohaline region, with the salinity ranging from 5 to 26 ~~psu~~psu/kg/kg. The highest and
702 lowest salinities are both increased when compared to Case 1, with a reduced magnitude
703 of salinity change in a tidal cycle. The salinity variation pattern remains similar to that
704 in Case 1, with minimum salinities occurring just before neap tides, and maximum
705 salinities after neap tides, but occur closer to spring tides. The asymmetry of quick
706 increase from neap to spring but gradual decrease afterwards is still clear.

707 When entering into the sub-estuary, the salinity variation at S3 in the middle of the

708 sub-estuary shows a more in-phase relationship between salinity and tidal range (Figs.
709 11c and 12c). The maximum salinities occur closer to spring tides whereas the
710 minimum salinities still occur just before neap tides. In the upstream region of the sub-
711 estuary (Figs. 11d and 12d), the phase relationship between salinity and tidal range is
712 also an in-phase one. Combined with the situation at the S1 Station, it indicates that the
713 variations of salinity at stations S4 and S1 are more synchronous. This largely explains
714 the observed phenomenon that under more drought conditions, the salinity variations at
715 the Second Water Plant kept pace with those at the Dahu Station (Section 3.1).

716

717 **5.3 Limitations and implications of this study**

718

719 In this study, we focus on the phase relationship between the variations of salinity
720 and tidal range, both in a sub-estuary and the main estuary. The salinity variations along
721 the sub-estuary are revealed to be associated with the salinity dynamics in the main
722 estuary, linked by the salinity variations at the confluence between the main estuary and
723 the sub-estuary. In a spring-neap tidal cycle, even when the salinity at the confluence is
724 a little lower during the spring tide than that during the neap tide, the higher horizontal
725 dispersion and decreased freshwater release at the head of the sub-estuary during the
726 spring tide can pump more saline water from the confluence into the middle and
727 upstream of the sub-estuary, and cause the salinities there to be higher than during the
728 neap tide. In this way, the salinity variations at areas farther away from the confluence
729 become more synchronous with the tidal range.

730 However, this study did not consider the effect of winds and waves, as shown to

731 be important in previous studies such as Gong et al. (2018). The variations of salinity
732 in the period of 5-8 days should be related to the wind effects and await future
733 exploration. The effect of sea level change outside the main estuary was also not
734 examined in detail, though it can be intrinsically linked to the effect of winds and waves.
735 Finally, we did not explore a full parameter space of river discharge, tidal range, and
736 bathymetry situations, and thus can not give a synthesis of the sub-estuary salt intrusion
737 dynamics at this time.

738 Despite all these limitations, this study has implications for studying salt intrusion
739 dynamics in sub-estuaries, which are influenced by both the hydrodynamics inside the
740 sub-estuary and the salt dynamics in the main estuaries. It is also of importance for
741 providing a scientific basis for salt intrusion mitigation in the region. For example, salt
742 intrusion in the sub-estuary is not only impacted by the river discharge from the head
743 of the sub-estuary itself but also largely affected by the salt dynamics in the main estuary.
744 In this respect, apart from releasing more freshwater from the upstream in the sub-
745 estuary, measures to control the salinity variations at the confluence between the main
746 estuary and the sub-estuary also need to be taken into consideration. This may involve
747 implementing engineering solutions such as the construction of barriers or gates to
748 regulate the inflow of saltwater from the main estuary into the sub-estuary. Additionally,
749 the management of water withdrawals and releases in the sub-estuary and main estuary
750 needs to be optimized by taking the estuarine system as a whole. Overall, a
751 comprehensive and coordinated approach is necessary to effectively mitigate salt
752 intrusion in sub-estuaries.

753

754 **6. Summary and conclusions**

755

756 From 2021 to 2022, under the influence of an extended La Nina event, the Pearl
757 River Delta region in China experienced a prolonged extreme drought condition, and
758 the sub-estuary (East River estuary) also suffered greatly from the enhanced salt
759 intrusion. To identify the characteristics of the salt intrusion in the sub-estuary, and to
760 explore the underlying physics in controlling the spatio-temporal variations of the salt
761 intrusion, we collected observation data and conducted numerical simulations for
762 idealized estuarine bathymetry, and used analytical solutions for the ~~subtidal-tidally-~~
763 averaged salinity variations in the sub-estuary. The observation data showed that the
764 salinity variation in the main estuary usually led that of the tidal range, and the
765 asymmetry between salinity rise and fall in a fortnightly timescale was prominent.
766 However, in the upstream region of the sub-estuary, the salinity variation was in phase
767 with that of the tidal range, and the salinity rise and fall were more symmetrical. The
768 idealized model simulations and the analytical solution both reproduced these
769 phenomena.

770 We note that under drought conditions, the river-tide interaction played a role in
771 the in-phase relationship between the salinity and tidal range upstream region of the
772 sub-estuary. The salinity variation in the middle and upstream regions of the sub-
773 estuary can keep pace with that of the tidal range. The analytical results show that the
774 horizontal dispersion scaling with tidal strength can largely reproduce the changes in
775 phase relationship between salinity and tidal range in the sub-estuary. We conclude that

776 both the changes in horizontal dispersion and the river-tide interaction in modulating
777 the freshwater release are responsible for the in-phase relationship between the salinity
778 and tidal range in the middle and upstream regions of the sub-estuary.

779 This study is of help in the investigation of salt dynamics in sub-estuaries
780 connected to main estuaries, and of implications for mitigating salt intrusion problems
781 in the regions suffered from enhanced salt intrusion by climate change and human
782 interventions.

783

784 **Data availability:** The observation data can be downloaded from the website
785 <http://www.pearlwater.gov.cn/>. The numerical data is available upon request to the
786 corresponding author.

787

788 **Declaration of competing interest**

789 The contact author has declared that none of the authors has any competing
790 interests.

791

792 **CRedit authorship contribution statement**

793 **Zhongyuan Lin:** Data collection, wavelet analysis, Writing - original draft, Writing -
794 review & editing. **Guang Zhang:** numerical modeling, Writing - review & editing.

795 **Huazhi Zou:** Writing-review & editing, funding acquisition. **Wenping Gong:**
796 Conceptualization, Methodology, Writing-review & editing, funding acquisition.

797

798 **Acknowledgments**

799

800 This research was funded by the National Natural Science Foundation of China
801 (grant numbers 42276169, 42306015) and The Science and Technology Innovation
802 Program from Water Resources of Guangdong Province (2023-01). Savenije, H.H.G.
803 at the Delft University of Technology and another anonymous reviewer are greatly
804 appreciated for their constructive comments and suggestion to improve this manuscript.
805 We would also like to thank the editor Huthnance, J. for his great insights in the
806 scientific issues raised in this manuscript.

807

808 **Supplement:**

809

810 We present the longitudinal profiles of subtidal-tidally-averaged current and salinity
811 along the channels in the main estuary and the sub-estuary during typical spring and
812 neap tides. Fig. S1 is for the dry condition with 1500 m³/s at the head of the main estuary,
813 and Fig. S2 for the extremely dry condition with 500 m³/s released at the head of the
814 main estuary.

815

816 **References**

817

818 Bowden, K. F., 1965. Horizontal mixing in the sea due to a shearing current. Journal of

819 Fluid Mechanics 21, 83-95. <https://doi.org/10.1007/BF00167972>

820 Bowen, M., Geyer, W.R., 2003. Salt transport and the time-dependent salt balance of a

821 partially stratified estuary. Journal of Geophysical Research 108(C5), 3185.

822 <https://doi.org/10.1029/2001JC001231>.

823 Buschman, F. A., Hoitink, A. J. F., Vegt., M. V. D., 2009. Subtidal water level variation

824 controlled by river flow and tides. Water Resources Research 45(10), W10420.

825 <https://doi.org/10.1029/2009WR008167>

826 Cai, H., Savenije, H.H.G., Zuo, S., Jiang, C., Chua, V.P., 2015. A predictive model for
827 salt intrusion in estuaries applied to the Yangtze estuary. *Journal of Hydrology* 529,
828 1336-1349. <https://doi.org/10.1016/j.jhydrol.2015.08.050>

829 Chapman, D. C., 1985. Numerical Treatment of Cross-Shelf Open Boundaries in a
830 Barotropic Coastal Ocean Model. *Journal of Physical Oceanography* 15(8), 1060-
831 1075. [https://doi.org/10.1175/1520-0485\(1985\)015<1060:NTOCSO>2.0.CO;2](https://doi.org/10.1175/1520-0485(1985)015<1060:NTOCSO>2.0.CO;2)

832 Chen S.-N., 2015. Asymmetric Estuarine Responses to Changes in River Forcing: A
833 Consequence of Nonlinear Salt Flux. *Journal of Physical Oceanography* 45(11),
834 2836-2847. <https://doi.org/10.1175/JPO-D-15-0085.1>

835 Dong, L., Su, J., Wong, L., Cao, Z., Chen, J.-C., 2004. Seasonal variation and dynamics
836 of the Pearl River plume. *Continental Shelf Research* 24(16), 1761-1777.
837 <https://doi.org/10.1016/j.csr.2004.06.006>

838 [Du, J., Park, K., 2019. Estuarine salinity recovery from an extreme precipitation event:
839 Hurricane Harvey in Galveston Bay. *Science of the Total Environment* 670, 1049-
840 1059. <https://doi.org/10.1016/j.scitotenv.2019.03.265>](#)

841 Flather, R. A., 1976. A tidal model of the northwest European continental shelf. ~~A tidal~~
842 ~~model of the northwest European continental shelf.~~ [Mémoires Société Royale des](#)
843 [Sciences de Liège Mem. Soc. R. Sci. Liege](#) 10(6), 141-164.

844 Gong, W., Shen, J., 2011. The response of salt intrusion to changes in river discharge
845 and tidal mixing during the dry season in the Modaomen Estuary, China.
846 *Continental Shelf Research*, 31, 769–788.

- 847 <https://doi.org/10.1016/j.csr.2011.01.011>
- 848 Gong, W., Lin, Z., Chen, Y., Chen, Z., Zhang, H., 2018. Effect of winds and waves on
849 salt intrusion in the Pearl River estuary. *Ocean Science* 14(1), 139-159.
850 <https://doi.org/10.5194/os-14-139-2018>
- 851 Gong, W., Chen, L., Zhang, H., Yuan, L., Chen, Z., 2020. Plume Dynamics of a Lateral
852 River Tributary Influenced by River Discharge From the Estuary Head. *Journal of*
853 *Geophysical Research: Oceans.* [doi:](https://doi.org/10.1029/2019JC015580)
854 [10.1029/2019JC015580](https://doi.org/10.1029/2019JC015580).<https://doi.org/10.1029/2019JC015580>
- 855 Gong, W., Lin, Z., Zhang, H., Lin H., 2022. The response of salt intrusion to changes
856 in river discharge, tidal range, and winds, based on wavelet analysis in the
857 Modaomen estuary, China. *Ocean & Coastal Management* 219, 106060.
858 <https://doi.org/10.1016/j.ocecoaman.2022.106060>
- 859 Haidvogel, D. B., Arango, H. G., Hedstrom, K., Beckmann, A., Malanotte-Rizzoli, B.,
860 Shchepetkin, A., F., 2000. Model evaluation experiments in the North Atlantic
861 Basin: Simulations in nonlinear terrain-following coordinates. *Dynamics of*
862 *Atmospheres and Oceans* 32(3-4), 239-281. [https://doi.org/10.1016/S0377-](https://doi.org/10.1016/S0377-0265(00)00049-X)
863 [0265\(00\)00049-X](https://doi.org/10.1016/S0377-0265(00)00049-X)
- 864 Haywood, D., Welch, C. S., Hass, L. W., 1982. York River destratification: an estuary-
865 sub-estuary interaction. *Science* 216, 1413-1414.
866 <https://doi.org/10.1126/science.216.4553.1413>
- 867 Hong, B., Liu, Z., Shen, J., Wu, H., Gong, W., Xu, H., Wang, D., 2020. Potential
868 physical impacts of sea-level rise on the Pearl River Estuary, China. *Journal of*

869 Marine Systems 201, 103245. <https://doi.org/10.1016/j.jmarsys.2019.103245>

870 Hu, J., Li, S., Geng, B., 2011. Modeling the mass flux budgets of water and suspended
871 sediments for the river network and estuary in the Pearl River Delta, China. *Journal*
872 *of Marine Systems* 88(2), 252-266. <https://doi.org/10.1016/j.jmarsys.2011.05.002>

873 Jia, L., Luo, Z., Yang, Q., Ou, S., Lei, Y., 2006. The impact of massive sand mining on
874 the morphology and tidal dynamics in the downstream of East River and the East
875 River Delta (In Chinese). *Acta Geographica Sinica* 2006(09), 985-994.

876 Liu, B., Yan, S., Chen, X., Lian, Y., Xin, Y., 2014. Wavelet analysis of the dynamic
877 characteristics of saltwater intrusion - A case study in the Pearl River Estuary of
878 China. *Ocean & Coastal Management* 95, 81-92.
879 <https://doi.org/10.1016/j.ocecoaman.2014.03.027>

880 MacCready, P., Geyer, W. R., 2010. Advances in estuarine physics. *Annual Review of*
881 *Marine Science* 2(1), 35-58. [https://doi.org/10.1146/annurev-marine-120308-](https://doi.org/10.1146/annurev-marine-120308-081015)
882 [081015](https://doi.org/10.1146/annurev-marine-120308-081015).

883 Mao, Q., Shi, P., Yin, K., Gan, J., Qi, Y., 2004. Tides and tidal currents in the Pearl River
884 Estuary. *Continental Shelf Research* 24(16), 1797-1808.
885 <https://doi.org/10.1016/j.csr.2004.06.008>

886 Okubo, A., 1973. Effect of shoreline irregularities on streamwise dispersion in estuaries
887 and other embayments. *Netherlands Journal of Sea Research* 6, 213-224.
888 [https://doi.org/10.1016/0077-7579\(73\)90014-8](https://doi.org/10.1016/0077-7579(73)90014-8)

889 Orlandi, I., 1976. A simple boundary condition for unbounded hyperbolic flows.
890 *Journal of Computational Physics* 21(3), 251-269.

891 [http://dx.doi.org/10.1016/0021-9991\(76\)90023-1](http://dx.doi.org/10.1016/0021-9991(76)90023-1)

892 Payo-Payo, M., Bricheno, L. M., Dijkstra, Y. M., Cheng, W., Gong, W., Amoudry, L.
893 O., 2022. Multiscale temporal response of salt intrusion to transient river and
894 ocean forcing. *Journal of Geophysical Research: Oceans* 127, e2021JC017523.
895 <https://doi.org/10.1029/2021JC017523>.

896 Ralston, D. K., Geyer, W. R., Lerczak J. A., 2010. Structure, variability, and salt flux in
897 a strongly forced salt wedge estuary, *J. Geophys. Res.*, 115, C06005,
898 [doi:10.1029/2009JC005806](https://doi.org/10.1029/2009JC005806).

899 Ralston, D. K., Geyer, W. R., 2019. Response to channel deepening of the salinity
900 intrusion, estuarine circulation, and stratification in an urbanized estuary. *Journal*
901 *of Geophysical Research: Oceans* 124, 4784–4802.
902 <https://doi.org/10.1029/2019JC015006>

903 Savenije, H.H.G., 2012. Salinity and tides in alluvial estuaries. Second Edition
904 <www.salinityandtides.com>.

905 Shchepetkin, A. F., McWilliams, J. C., 2005. The regional ocean modeling system
906 (ROMS): A split-explicit, free-surface, topography-following coordinates oceanic
907 model. *Ocean Modeling* 9, 347–404.
908 <https://doi.org/10.1016/j.ocemod.2004.08.002>

909 Simpson, J.H., Brown, J., Matthews, J.P., Allen, G., 1990. Tidal straining, density
910 currents, and stirring in the control of estuarine stratification. *Estuaries* 13 (2),
911 125–132.

912 Smagorinsky, J., 1963. General Circulation Experiments with the Primitive Equation,

913 Part 1, the Basic Experiment. *Monthly Weather Review* 91(3), 99-164.
914 <http://dx.doi.org/10.1175/1520-0493>

915 Spinoni, J., Naumann, G., Carrao, H., Barbosa, P., Vogt, J., 2014. World drought
916 frequency, duration, and severity for 1951–2010. *International Journal of*
917 *Climatology Int. J. Climatol.* 34(8), 2792–2804. <https://doi.org/10.1002/joc.3875>

918 Stommel, H., Farmer, H. G., 1952. On the nature of estuarine circulation: part I
919 (chapters 3 and 4). Woods Hole Oceanographic Institution.

920 Umlauf, L., Burchard, H., 2003. A generic length-scale equation for geophysical
921 turbulence models. *Journal of Marine Research* 61(2), 235-365.
922 <https://doi.org/10.1357/002224003322005087>

923 Uncles, R. J., Stephens, J. A., 2010. Turbidity and sediment transport in a muddy sub-
924 estuary. *Estuarine, Coastal and Shelf Science* 87(2), 213-224.
925 <https://doi.org/10.1016/j.ecss.2009.03.041>

926 Warner, J. C., Sherwood, C. R., Arango, H. G., Signell, R. P., Butman, B., 2005.
927 Performance of four turbulence closure models implemented using a generic length
928 scale method. *Ocean Modeling* 8, 81–113.

929 Wei, X., Kumar, M., Schuttelaars, H.M., 2017. Three-dimensional salt dynamics in
930 well-mixed estuaries: influence of estuarine convergence, Coriolis, and bathymetry.
931 *Journal of Physical Oceanography* 47, 1843-1872.
932 <https://doi.org/10.1016/j.ocemod.2003.12.003>

933 Wong, L. A., Chen, J. C., Xue, H., Dong, L. X., Su, J. L., Heinke, G., 2003. A model
934 study of the circulation in the Pearl River Estuary (PRE) and its adjacent coastal

935 waters: 1. Simulations and comparison with observations. *Journal of Geophysical*
936 *Research* 108(C5). <https://doi.org/10.1029/2002jc001451>

937 Wu, Z. Y., Saito, Y., Zhao, D. N., Zhou, J. Q., Cao, Z. Y., Li, S. J., 2016. Impact of
938 human activities on subaqueous topographic change in Lingding Bay of the Pearl
939 River estuary, China, during 1955-2013. *Scientific Reports* 6, 37742.
940 <https://doi.org/10.1038/srep37742>

941 Yellen, B., Woodruff, J. D., Ralston, D. K., MacDonald, D. G., Jones, D. S., 2017. Salt
942 wedge dynamics lead to enhanced sediment trapping within side embayments in
943 high-energy estuaries. *Journal of Geophysical Research: Oceans* 122(3), 2226-
944 2242. <https://doi.org/10.1002/2016JC012595>

945 Zhang, P., Yang, Q., Wang, H., Cai, H., Liu, F., Zhao, T., Jia, L., 2021. Stepwise
946 alterations in tidal hydrodynamics in a highly human-modified estuary: The roles
947 of channel deepening and narrowing. *Journal of Hydrology* 597, 126153.
948 <https://doi.org/10.1016/j.jhydrol.2021.126153>

949 Zimmerman, J. T. F., 1986. The tidal whirlpool: A review of horizontal dispersion by
950 tidal and residual currents. *Netherlands Journal of Sea Research* 20, 133-154.
951 [https://doi.org/10.1016/0077-7579\(86\)90037-2](https://doi.org/10.1016/0077-7579(86)90037-2)
952

953

954 **Figure Captions:**

955

956 Fig.1. a) The East River estuary; b) Map of the Pearl River Delta and the
957 locations of hydrological and water level stations.

958 Fig. 2. Geometry and bathymetry of the idealized model domain: a)for the
959 whole domain; b)zoom in for the area of concern. The origin of the coordinates is in
960 the middle of the main estuary mouth. The longitudinal sections in the main and sub-
961 estuary are shown as dashed lines, and the cross-sections inside the sub-estuary are
962 shown as color solid lines. The locations of several stations are indicated.

963 Fig.3. Timeseries of: a) Daily maximum salinity at the Second Water Plant; b)
964 Total duration period with salinity exceeding 0.5 ~~psu~~psu/kg/kg for each month; c)
965 Monthly river discharge at Boluo station (upstream of the East River); d) Monthly
966 river discharge at Wuzhou station (upstream of the West River); e) Monthly river
967 discharge at Shijiao station (upstream of the North River).

968 Fig. 4 Wavelet analysis of the salinity at the Second Water Plant.

969 Fig. 5. Timeseries of: a) Daily maximum salinity at the Second Water Plant; b)
970 Daily river discharge at Boluo station; c) Daily maximum tidal range at Sishengwei
971 Station; d) Daily maximum salinity at Dahu Station; e) Daily mean sea level at Shibi
972 Station.

973 Fig. 6. Cross-wavelet analysis of (a) between the salinity at Dahu and the tidal
974 range at Sishengwei; (b) between the salinity at the Second Water Plant and the tidal
975 range at Sishengwei; (c) between the salinity at the Second Water plant and the river

976 discharge at the Boluo Station; (d) between the salinity at the Second Water plant and
977 that at the Dahu Station.

978 Fig. 7. Timeseries of: a) tidal range at the mouth of the main estuary; b) salt
979 intrusion length along the longitudinal section of the main estuary; c) salt intrusion
980 length along the longitudinal section of the sub-estuary.

981 Fig. 8. Timeseries of water level at the confluence and surface salinity a) at S1
982 Station in the main estuary; b) at S2 station (the confluence); c) at S3 station in the
983 middle of the sub-estuary; d) at S4 station in the upstream region of the sub-estuary.

984 Fig. 9. The results of the analytical solution of salinity variations along the sub-
985 estuary. a) tidal range at the mouth of the sub-estuary; b), c), and d) are ~~tidally-~~
986 ~~averagedsubtidal~~ salinity variations at S2, S3, and S4 stations.

987 Fig. 10. Timeseries of: a) tidal range at the mouth of the sub-estuary; b) salt flux
988 at the cross-section near the mouth of the sub-estuary; c) freshwater flux at the cross-
989 section in the upstream region of the sub-estuary.

990 Fig. 11. Timeseries of water level at the confluence and surface salinity under
991 the extremely lower river discharge in the main estuary at stations of: a) S1; b) S2; c)
992 S3; d) S4.

993 Fig. 12. The results of the analytical solution of salinity variations along the sub-estuary
994 under extremely dry conditions. a) tidal range at the mouth of the sub-estuary; b),
995 c), and d) are ~~tidally-averagedsubtidal~~ salinity variations at S2, S3, and S4 stations.